Valency and affinity control of aptamer-conjugated nanoparticles for selective cancer cell targeting

Journal of Controlled Release 355 (2023) 228–237

Contents lists available at ScienceDirect

Journal of Controlled Release

journal homepage: www.elsevier.com/locate/jconrel

Valency and affinity control of aptamer-conjugated nanoparticles for selective cancer cell targeting

Laura Woythe [a], David Porciani [b], Tessa Harzing [a], Stijn van Veen [a], Donald H. Burke [b,c], Lorenzo Albertazzi [a,d,*]

[a] Department of Biomedical Engineering, Institute for Complex Molecular systems (ICMS), Eindhoven University of Technology, Netherlands
[b] Department of Molecular Microbiology & Immunology, School of Medicine, University of Missouri, Columbia, USA
[c] Department of Biochemistry, University of Missouri, Columbia, USA
[d] Institute of Bioengineering of Catalonia (IBEC), the Barcelona Institute of Science and Technology (BIST), Spain

ARTICLE INFO

Keywords:
Tumor targeting
Silica-supported lipid bilayers
Multivalency
Nanoparticle targeting
Aptamer avidity and affinity

ABSTRACT

Nanoparticles (NPs) are commonly functionalized using targeting ligands to drive their selective uptake in cells of interest. Typical target cell types are cancer cells, which often overexpress distinct surface receptors that can be exploited for NP therapeutics. However, these targeted receptors are also moderately expressed in healthy cells, leading to unwanted off-tumor toxicities. Multivalent interactions between NP ligands and cell receptors have been investigated to increase the targeting selectivity towards cancer cells due to their non-linear response to receptor density. However, to exploit the multivalent effect, multiple variables have to be considered such as NP valency, ligand affinity, and cell receptor density. Here, we synthesize a panel of aptamer-functionalized silica-supported lipid bilayers (SSLB) to study the effect of valency, aptamer affinity, and epidermal growth factor receptor (EGFR) density on targeting specificity and selectivity. We show that there is an evident interplay among those parameters that can be tuned to increase SSLB selectivity towards high-density EGFR cells and reduce accumulation at non-tumor tissues. Specifically, the combination of high-affinity aptamers and low valency SSLBs leads to increased high-EGFR cell selectivity. These insights provide a better understanding of the multivalent interactions of NPs with cells and bring the nanomedicine field a step closer to the rational design of cancer nanotherapeutics.

1. Introduction

Selective cancer NP targeting is highly desired to direct therapeutics to their site of action while minimizing off-target effects [1]. NP selectivity is commonly achieved by decorating the NP surface with targeting ligands that interact specifically with a biomarker or receptor of interest. This strategy is specifically attractive for selective cancer therapeutics due to the overexpression of some receptors in cancer cells. However, common targets pursued in cancer nanomedicine are also present in healthy tissues, complicating selective targeting of NPs. For example, the epidermal growth factor receptor (EGFR) is a common cancer therapeutic target, but it is also expressed in cells of epithelial origin, such as the skin, gastrointestinal- and respiratory organs [2]. Notably, there are no clinically approved targeted NPs so far. Thus, circumventing adverse side effects caused by on-target/off-tumor targeting is crucial for developing successful targeted NPs [3].

Multivalent particles with multiple copies of targeting ligand on the NP surface are sometimes used for an increase in specificity, but theoretical studies have shown that it can lead to an increase in selectivity as well. NPs that bind monovalently to a target do not discriminate between surfaces with different receptor densities. However, multivale nt NPs with multiple targeting ligands have been shown to bind heterogeneously depending on the surface receptor density [4,5]. The regime where the bound fraction correlates with receptor density is called “super-selectivity”, and it can approach an on-off binding behavior [6]. This increased selectivity can be achieved using engineered weakly-binding NP ligands, such as glycans, peptides, or aptamers, that increase the overall NP binding affinity by engaging in multiple ligand-receptor bonds [7]. Thus, the binding is strong at high receptor density and too weak at low receptor density, reducing potential off-cancer

* Corresponding author at: Department of Biomedical Engineering, Institute for Complex Molecular systems (ICMS), Eindhoven University of Technology, Netherlands.
E-mail address: L.albertazzi@tue.nl (L. Albertazzi).

https://doi.org/10.1016/j.jconrel.2023.01.008
Received 8 August 2022; Received in revised form 16 December 2022; Accepted 4 January 2023
Available online 8 February 2023

interactions. Valuable insights on super-selectivity have been gained from model systems using DNA-functionalized materials, emphasizing the importance of valency and affinity of the multivalent interactions [8–10]. However, studies investigating the interplay among NP valency, ligand affinity, and receptor density to maximize selectivity in cells are scarce due to the challenging control of these parameters. Optimal ligand density is often explored in NP targeting [11], while ligand affinity and receptor density often require sophisticated engineering of ligands [12] and cells [13].

Here, we use aptamer-functionalized silica-supported lipid bilayers (SSLB), which are silica nanoparticles covered by a lipid bilayer, to study the interplay between NP valency, aptamer affinity and EGFR expression on the targeting specificity and super-selectivity in a panel of breast cancer cell lines. Aptamers are small, flexible, and non-immunogenic ligands that can be rationally engineered to have high specificityfor cell surface receptors [14]. Furthermore, their ease of sequence engineering and rapid synthesis allows creating aptamer variants with different affinity. Due to the numerous advantages, aptamer-NP conjugates have been developed to improve targeted cancer therapy [15]. In this regard, SSLBs are attractive nanocarriers due to the favorable combination of silica and lipid bilayer properties [16], conferring biocompatibility, improved stability, and the controllable aptamer surface functionalization via cholesterol-based linkers [17].

First, SSLB functionalization with aptamers was confirmed by single-molecule localization microscopy (SMLM), which allows the quantification of interparticle ligand heterogeneities in the same particle formulation [7]. Subsequently, a panel of breast cancer cell lines with different EGFR expression densities on the cell surfaces was investigated to assess whether our SSLBs can selectively target high EGFR expressing cells. We show that by tuning the aptamer affinity and SSLB valency, the super-selectivity towards high-expressing EGFR cells can be optimized. Furthermore, strategies to decrease targeting towards low EGFR expressing cells are discussed. Our results demonstrate that choosing high valency particles can lead to non-specific binding in cells of low EGFR density and reduced particle selectivity, whereas using high-affinity ligands in low valency NPs reduced non-specific binding while retaining selective interactions with target cells. We emphasize the importance of a rational design of affinity and valency of NPs to increase selective cancer cell targeting with the final aim of translating targeted NPs to the clinic.

2. Materials and methods

2.1. Materials

Fluorescent silica NPs (Sicastar-greenF, plain) of 100 nm radius were obtained from Micromod Partikeltechnologie GmbH. The 1,2-dioleoyl-*sn*-glycero-3-phosphocholine (DOPC), extrusion filter supports (10 mm) and PC membranes for extrusion were purchased from Avanti Polar lipids. DMEM (high glucose, no phenol red), Penicillin-Streptomycin, Fetal Bovine Serum (FBS, qualified), Trypsin-EDTA (0.5%), 4-(2-hydroxyethyl)-1-piperazineethanesulfonic acid (HEPES) buffer (1 M), Vibrant DiI solution, streptavidin, biotinylated bovine serum albumin (BSA-biotin) and Nunc cell culture flasks were obtained from Thermo Fisher Scientific. Cysteamine, glucose oxidase, catalase from bovine liver, magnesium chloride, phosphate buffered saline (PBS), Tris-EDTA buffer and chloroform were purchased from Merck Life Science. Sodium chloride (NaCl) was obtained from Sanal. MDA-MB-231 and MCF-7 cells were kindly provided by Prof. Jaap den Toonder (Eindhoven University of Technology). MDA-MB-468 cells (HTB-132), BT-474 cells (HTB-20), BT-20 cells (HTB-19), Eagle's Minimum Essential Medium (EMEM) and DMEM F-12 were purchased from ATCC. Alexa Fluor 647 AffiniPure Goat Anti-Mouse antibody was purchased from Jackson Immunoresearch. The μ-slide 8-well and 18-well glass bottom chambered coverslips (#1,5H) were obtained from Ibidi. Cholesterol-DNA linkers were ordered from Eurogentec. DNA oligos for aptamer synthesis and DNA-dye conjugated oligos (DNA-AF647 and DNA-atto647N) were purchased from Integrated DNA Technologies (IDT). A detailed list of the DNA sequences can be found in Supplementary Table S1. Urea, sodium acetate and TE buffer were purchased from Sigma-Aldrich. ATP, GTP, 2′-fluoro modified CTP and 2′-fluoro modified UTP were purchased from TriLink Biotechnologies.

2.2. Synthesis of SSLBs

Silica-supported DOPC lipid bilayers were synthesized as previously described [18]. First, small unilamellar DOPC vesicles were formed via thin film hydration and extrusion. Subsequently, 200 μL of 10 mM DOPC lipid stock was dissolved in chloroform, after which the chloroform solvent was evaporated by vortexing under nitrogen flow. After solvent evaporation, a thin lipid film was formed on the glass vial walls which was rehydrated using 1 mL of 10 mM HEPES and 50 mM NaCl buffer (pH 7.4) and vortexed for 2 min. The resulting vesicle suspension was extruded using an Avanti Mini Extruder 21 times through a 200 nm filter, 21 times through a 100 nm filter and 21 times through a 50 nm filter all at room temperature. Next, SSLBs were formed by mixing 400 μL of vesicle suspension with 20 μL of sicastar silica nanoparticles (stock 50 mg/mL) and 980 μL 10 mM HEPES and 50 mM NaCl buffer for 1 h at 22 °C under shaking in a ThermoMixer®. Finally, the SSLBs were washed thrice via centrifugation at 16000*g* for 15 min to remove free lipid vesicles and redispersed in 10 mM HEPES and 50 mM NaCl. SSLB were stored at 4 °C and used within one week.

2.3. Size and charge characterization of NPs

DOPC vesicles, silica NPs and SSLBs were measured via dynamic light scattering (DLS) and laser Doppler electrophoresis using a Malvern Zetasizer Nano ZS (Malvern Instruments) to determine their size and zeta potential. For size measurements, 20 μL DOPC suspension, 20 μL 1 mg/mL silica NPs or 20 μL 1 mg/mL SSLB in 10 mM HEPES and 50 mM NaCl were added to a ZEN2112 cuvette and measured in triplicate, with 10 runs for each measurement. For zeta potential measurements, 20 μL DOPC suspension, 20 μL silica NPs stock or 50 μL SSLB were diluted in MilliQ water and measured in triplicate.

2.4. Annealing of cholesterol-DNA linkers

DNA oligo stocks were resuspended at 100 μM in Tris-EDTA buffer. A detailed list of DNA linker sequences is reported in Table S1 of the Supporting information. Annealing of cholesterol-DNA sequences to obtain the double-cholesterol DNA linker was performed by mixing 100 μM cholesterol-DNA (base) and 100 μM cholesterol-DNA (sticky end) in the presence of 5 mM magnesium chloride and 10 mM HEPES 50 mM NaCl buffer for 1 h at 25 °C to achieve a final concentration of 1 μM chol-DNA with a 3′ single-stranded overhang. For dSTORM imaging, cholesterol-DNA linkers with a 3′ single-stranded overhang were annealed to a complementary DNA-AF647 sequence by mixing cholesterol-DNA with DNA-AF647 at a 1:1 M ratio for 1 h at 25 °C. For imaging, SSLBs were functionalized with a small amount of cholesterol-DNA-biotin by mixing cholesterol-DNA with DNA-biotin instead of DNA-AF647 at a 1:1 M ratio for 1 h at 25 °C.

2.5. dSTORM imaging and analysis of SSLB ligands

For dSTORM imaging, SSLBs were incubated with various amounts of cholesterol-DNA-AF647 linkers. Specifically, 50 μL of 2 mg/mL SSLBs were mixed with 2 μL (50 DNA/SSLB), 4 μL (100 DNA/SSLB), 8 μL (200 DNA/SSLB) or 16 μL (400 DNA/SSLB) of cholesterol-DNA-AF647 linkers (stock concentration 500 nM) for 1 h at 22 °C and diluted to a final concentration of 1 mg/mL with 10 mM HEPES 50 mM NaCl buffer. SSLBs were attached to a 18-well chambered coverslip for imaging via biotin-streptavidin interactions. The SSLBs were first incubated with 2

μL of 10 nM cholesterol-DNA-biotin.Then the chambered coverslips were incubated with a solution of 0.1 mg/mL BSA-biotin for 15 min, before being washed and incubated with 0.1 mg/mL streptavidin for 10 min and washed thrice with 10 mM HEPES 50 mM NaCl buffer. Afterwards, the 40 μL of 0.5 mg/mL SSLBs were added to the functionalized surface and incubated for 20 min. Finally, the non-attached SSLBs were washed away with 10 mM HEPES 50 mM NaCl buffer without letting the surface dry out. For dSTORM imaging, the buffer was exchanged with STORM buffer [19] (50 mM Tris pH 8, 10 mM NaCl, 10% *w/v* glucose, 50 mM cysteamine, 0.5 mg/mL glucose oxidase, 40 μg/mL catalase). A Nikon N-STORM microscope configured for TIRF imaging and equipped with a perfect focus system was used for dSTORM imaging. The AF647-labeled SSLBs were illuminated using a 647 nm laser (170 mW) and the sicastar®-greenF NPs were illuminated using a 488 nm laser (90 mW), with an adjusted TIRF angle to maximize the signal-to-noise ratio and without UV activation. A Nikon 100×, 1.4 NA oil immersion objective was used to collect the fluorescence signal, and was passed through a quad-band pass dichroic filter (97,335, Nikon) and recorded on an Andor EMCCD camera (ixon3) with pixel size 160 nm and a region of interest of 256 × 256 pixels. Samples were acquired for 20,000 frames at 30 ms exposure and 100% laser power for the 647 channel. The fluorescent silica NPs were used to identify the NP position and served as drift correction markers for the final image reconstruction by collecting one frame every 100 frames in the 488 channel at the same integration time and 5% laser power. A minimum of 200 NPs were imaged for each condition in minimum 3 distinct fields of view. The dSTORM images were analyzed with the Nikon NIS elements software (version 5.21.01). Single-molecule localizations were detected by Gaussian fitting, with a minimum intensity height threshold of 200 for the 647 channel and 150 for the 488 channel. Analysis was started at frame number 50 to eliminate non-blinking behavior in the beginning of the acquisition. Molecules detected in 5 consecutive frames were counted as a single fluorophore to prevent overcounting of localizations while molecules detected for more than 5 consecutive frames were removed. A density filter requiring a minimum of 10 localizations in a radius of 200 nm was applied to remove the background signal. The final localization list was imported and run through a custom MATLAB script to quantify the number of localizations for each NP. The code is extensively reported elsewhere [20]. Briefly, a mean shift clustering algorithm was applied to cluster the 488 localizations from the silica NPs. The bandwidth was adjusted to 200 nm and clusters with less than 10 localizations were discarded. Next, the number of localizations in the 647 channel were counted around each SSLB center, with a maximum counting radius of 300 nm. Aggregates with an unrealistic size were filtered out. The analysis output provided the number of localizations in the 647 channel per single SSLB, and this data was plotted using Origin 2020.

2.6. Aptamer generation

DNA oligos were resuspended at 100 μM in TE buffer (10 mM Tris-HCl pH 9.0, 1 mM EDTA). The 2′F-pyrimidine-modified RNA aptamers were generated as previously described via in vitro run-off transcription [21]. First, DNA templates were PCR amplified with primers that appended a T7 promoter (a detailed list of templates and primers can be found in Table S3 of the Supporting Information). Next, 2′F-pyrimidine-modified RNA aptamers were transcribed by run-off transcription reaction overnight at 37 °C using a recombinant mutant form of T7 RNA polymerase (Y639F mutant) generated in-house, in vitro transcription buffer (50 mM Tris-HCl pH 7.5, 15 mM MgCl2, 5 mM DTT, 4% *w/v* PEG4000 and 2 mM spermidine), and 2 mM of each ATP, GTP, 2′-fluoro modified CTP and 2′-fluoro modified UTP. RNA aptamers were purified through denaturing polyacrylamide gel electrophoresis (0.75 mm, 8% TBE-PAGE, 8 M urea) and bands corresponding to the expected product size were gel extracted and eluted while tumbling overnight in 300 mM pH 5.4 sodium acetate. Eluates were precipitated in ethanol, resuspended in TE buffer, and stored at −20 °C until further use. RNA aptamers included an extended tail sequence (5'-GCAGCAGCAGCAGCAGCA-3′) for subsequent hybridization with cholesterol-DNA-linkers. The full sequence of RNA aptamers can be found in Table S3 of the Supporting Information.

2.7. Functionalization of SSLB with aptamers

Cholesterol-DNA linkers with a 3'single-stranded overhang were annealed to a complementary aptamer tail sequence by mixing cholesterol-DNA with aptamers at a 1:1 M ratio for 1 h at 25 °C in the presence of 2.5 mM Magnesium chloride. Subsequently, 40 μL of SSLBs at 2 mg/mL stock concentration were incubated with various amounts of cholesterol-DNA-aptamer (corresponding to an estimated 50, 100, 200 and 400 DNA strands per SSLB) for 1 h at 22 °C. Afterwards, the SSLBs were sonicated for 5 min in a water bath. As a control, cholesterol-DNA was mixed with a non-targeting aptamer at low (50 DNA/SSLB) or high (400 DNA/ SSLB) valency. The resulting functionalized SSLBs were used the same day for cell targeting experiments.

2.8. Cell culture

MCF-7, MDA-MB-231 and MDA-MB-468 cells were cultured in DMEM (high glucose, no phenol red) supplemented with 10% FBS and penicillin-streptomycin (100 U/mL) at 37 °C and 5% CO_2. BT-474 cells were cultured in DMEM F-12 supplemented with 10% FBS and penicillin-streptomycin (100 U/mL) at 37 °C and 5% CO_2. BT-20 cells were cultured in EMEM supplemented with 10% FBS and penicillin-streptomycin (100 U/mL) at 37 °C and 5% CO_2.

2.9. SSLB targeting by flow cytometry

For SSLB targeting studies, cells were seeded in a 48-well plate at the following seeding densities based on their growth rate: MDA-MB-468, MDA-MD-231 and MCF-7 were seeded at 45000 cells/well and BT-20 and BT-474 cells were seeded at 90000 cells/ well. All cells were incubated for 48 h at 37 °C and 5% CO_2 after seeding. After 48 h, cells were incubated with 100 μg/mL SSLBs functionalized with aptamers diluted in DMEM without FBS for 1 h and 30 min at 37 °C and 5% CO_2. FBS was not used to avoid potential crowding effects of the protein corona, which could skew subsequent measurements. Subsequently, cells were washed once with PBS and detached from the well plate by 10 min incubation with trypsin at 37 °C. After cells successfully detached from the well plate, 300 μL of medium containing FBS was added to the cell suspension and cells were centrifuged once at 300*g* for 5 min. The cell supernatant was discarded and cells were resuspended in 300 μL BSA 1% diluted in PBS and kept refrigerated on ice until flow cytometry analysis. For each condition, a minimum of 20,000 cells were measured on a BD FACSCanto™ II configured for FITC detection (Fluorescent silica core). The amount of fluorescence is considered as a measure of uptake. While technically it measures both the particles associated to the cell as well as those internalized, it is assumed that anything bound strongly enough to remain after trypsinization would internalize eventually. Flow cytometry data was analyzed using FlowJo (version 10.7.1).

3. Results

Aptamer affinity and SSLB valency were investigated as essential features in the nanoparticle design to optimize super-selectivity towards cells expressing high EGFR densities (Fig. 1A). A summary of the SSLB design, characterization and cell selectivity is schematically represented in Fig. 1. Briefly, SSLBs consisting of non-porous silica particles covered by a fluid lipid bilayer were synthesized as previously described [18]. The presence of the lipid bilayer around silica NPs is essential for the subsequent aptamer incorporation and was confirmed using ensemble and single-particle characterization techniques (Fig. 1B). Next, the successful incorporation of targeting ligands was investigated using a

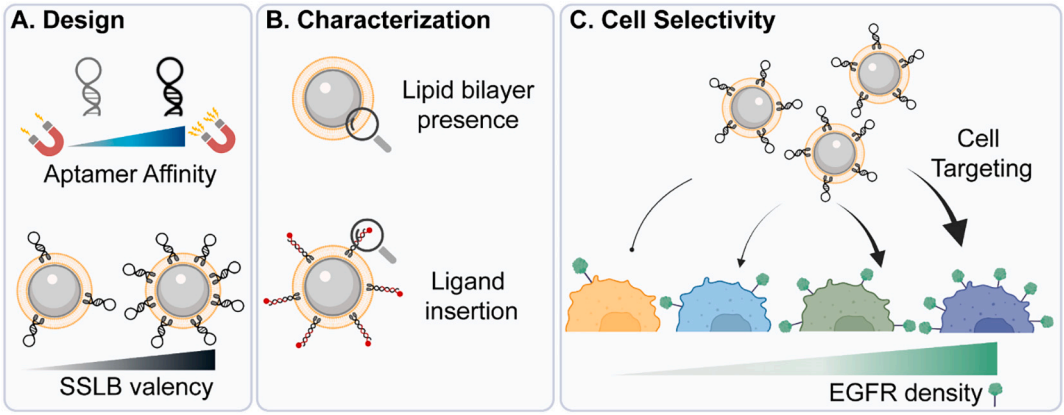

Fig. 1. Schematic representation of SSLB design, characterization, and cell selectivity towards a panel of breast cancer cell lines. A) SSLB design features. Aptamer affinity and NP valency control were investigated to optimize cell selectivity. B) After SSLB synthesis, the presence of the lipid bilayer around the silica NP core was confirmed, and successful ligand functionalization was quantified using super-resolution microscopy. C) Cell uptake of different SSLB formulations was investigated to determine the selectivity towards cancer cells of different EGFR cell surface densities.

SMLM technique that enables ligand quantification at a single-particle level (Fig. 1B). Finally, the targeting of SSLBs was evaluated in a panel of breast cancer cell lines with distinctive EGFR densities (Fig. 1C).

Ensemble and single-particle characterization techniques were used to confirm the presence of lipid bilayers around the silica NPs (Fig. 2). SSLB were first formed by incubating 200 nm diameter silica cores with small unilamellar vesicles (SUV) composed of the phospholipid 1,2-dioleoyl-*sn*-glycero-3-phosphocholine (DOPC) (Fig. 2A). During this process, the multiple DOPC vesicles rupture when interacting with the silica surface, causing the fusion of lipids into a lipid bilayer around the silica particle [22].

At the ensemble level, the hydrodynamic diameter and zeta potential were measured to confirm the bilayer presence around silica NPs using dynamic light scattering (DLS) and laser Doppler electrophoresis, respectively. We observed that the diameter of the SSLBs increased by approximately 35 nm compared to plain silica NPs (Fig. 2B), which can be attributed to the surrounding of silica NPs by the lipid bilayer coating. The size increase is slightly larger than expected (approximately 5 nm for the bilayer alone), which can be attributed to one of several reasons. Possibly there is slight particle aggregation caused by the new chemical surface environment, which would increase the average size. Another possible explanation lies in the shortcomings of light scattering. DLS does not necessarily measure size, but rather the hydrodynamic radius. Considering that the DOPC head groups now covering the particles are hydrophilic, this could feasibly lead to an increase in hydrodynamic radius. Additionally, the zeta potential of SSLB increases, which can be attributed to the negative silica surface charge being screened by the zwitterionic DOPC bilayer (Fig. 2C). Likely the particles are not fully covered, but with enough coverage the cholesterol-DNA can still intercalate in the lipid patches.

At a single-particle level, the presence of a lipid bilayer was qualitatively investigated by labeling the SSLBs with the lipophilic dye DiI and imaging the NP fluorescence using total internal reflection fluorescence (TIRF) microscopy (Fig. 2D). As a control, DiI dye was incubated with plain silica NPs. Fluorescent silica cores were used to detect the NP position and colocalize it with lipid marker DiI. We observed that DiI stained the lipid membrane around the silica cores of SSLB, while silica NPs alone were not stained. This specific lipid staining indicates that the lipid bilayer coverage is consistent through the formulation at a single-particle level. Confirming the lipid-bilayer presence is an important step for the subsequent incorporation of functional groups, such as targeting ligands, into the lipid bilayer. Here, ensemble and single-particle measurements confirmed the successful formation of SSLBs.

Incorporating ligands through cholesterol moieties is an attractive approach for ligand incorporation into SSLBs, as it avoids the use of complex chemistry that could hamper the ligand's functionality or conformation. We employed this strategy to functionalize SSLBs with varying amounts of anti-EGFR aptamers for selective cell targeting. For this functionalization approach, a double-stranded DNA linker was designed to have a 3′ single-stranded overhang (A) to attach aptamers bearing the complementary DNA sequence (anti-overhang A'). Additionally, the DNA linkers presented a double cholesterol anchor that was used to insert the construct into the lipid bilayer via hydrophobic interactions as seen in Fig. 3 and previously described by Rinaldin et al. [17]. Double cholesterol anchors have been reported to present a more stable binding to lipid bilayers than single cholesterol insertion [23,24].

To quantify the ligand incorporation into the SSLB, a fluorescent complementary DNA molecule (A') was attached to the cholesterol-DNA linker in place of the aptamer ligand using the same DNA hybridization strategy (between A and A') as explained above (Fig. 3). SSLBs incubated with different amounts of added cholesterol-DNA linkers were then quantified by direct Stochastic Optical Reconstruction Microscopy (dSTORM). dSTORM is a super-resolution microscopy technique that allows for the single-molecule quantification of fluorescent species with a resolution of around 20 nm, far below the diffraction limit of regular microscopy techniques [25]. For that purpose, a dSTORM compatible dye Alexa Fluor 647 (AF647) was attached to the single-strand DNA anti-overhang (A') (Fig. 3A). The final dSTORM image is a reconstruction of stochastically detected single-molecule localizations throughout a large number of acquired frames [26]. For each individual SSLB we calculated the number of dSTORM localizations detected, which is proportional to the number of dye molecules incorporated into the lipid bilayer through the cholesterol-DNA linkers.

Using dSTORM imaging we observed a linear increase in the number of localizations, which indicates a similar linear increase in incorporated ligands, with increased cholesterol-DNA linker addition to SSLB within the studied concentration range (approximately 50–400 chol-DNA molecules per SSLB added during the functionalization step according to theoretical calculations) (Fig. 3B and Fig. S1). Thus, high control over the number of incorporated ligands can be achieved in this concentration range. Fig. 3C displays a representative particle from the quantification in Fig. 3B, displayed as gaussian rendered localizations. The linear behavior is consistent with ensemble measurements performed using spectrophotometry (Fig. S2). The single-particle resolution of dSTORM allows for the quantification of possible heterogeneities in ligand functionalization of SSLBs. In all formulations, we observed high particle-to-particle heterogeneity in ligand number — resulting in the co-existence of SSLBs with a low or high amount of ligands in the same particle batch. Naturally, this heterogeneity would also be present in the cell interaction and internalization of the SSLBs.

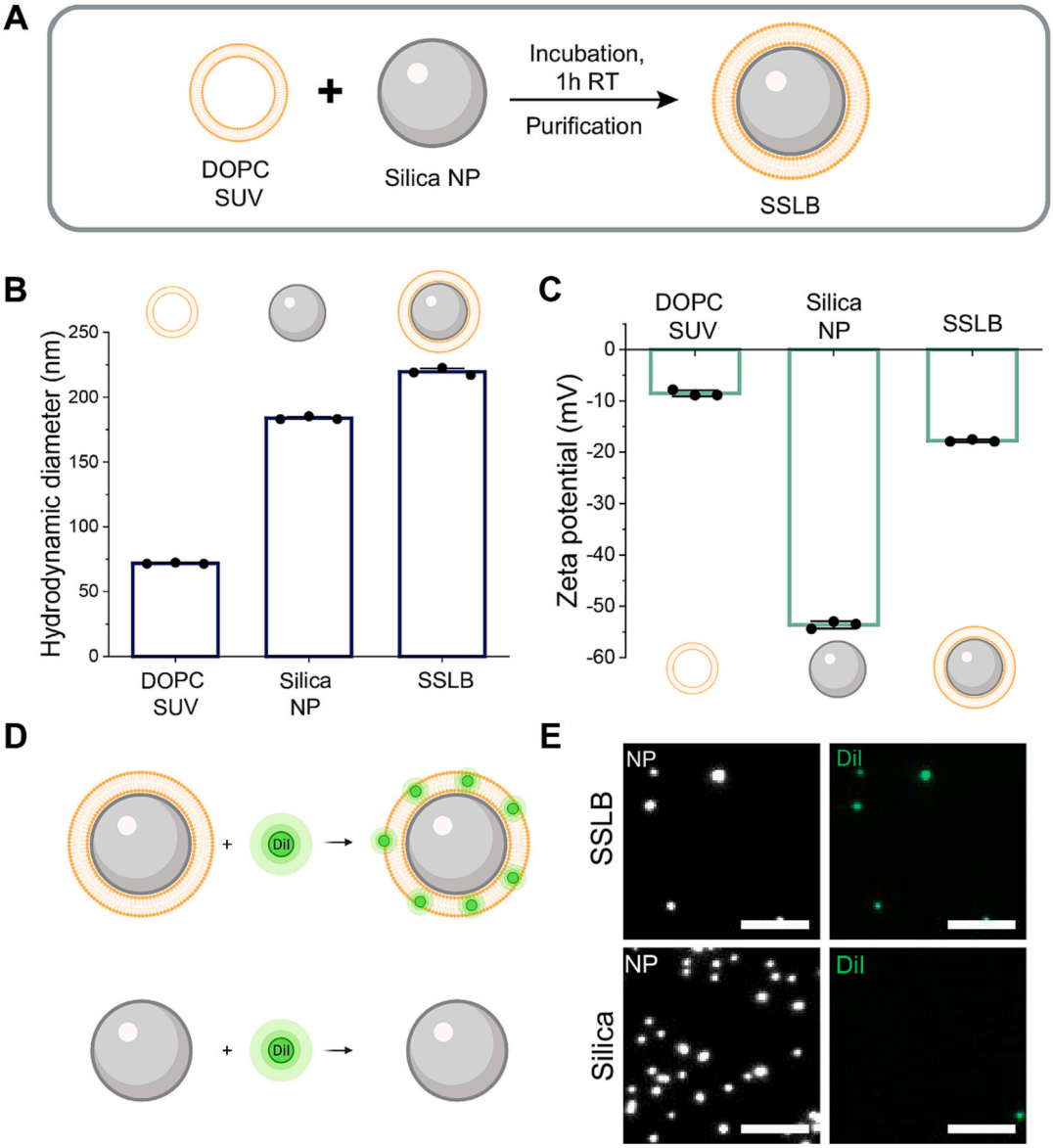

Fig. 2. Formation and characterization of silica-supported lipid bilayers (SSLB). A) Schematic representation of SSLB formation. B) Hydrodynamic diameter and C) zeta potential of DOPC small unilamellar vesicles (SUV), plain silica NPs and SSLB. D) Schematic illustration of DiI incorportation into SSLB to confirm the presence of lipid around silica NPs at a single-particle level. As a negative control, Dii was incubated with plain silica NPs. E) TIRF images of SSLB and plain silica NPs. Silica cores are labeled to detect the NP position (grey, silica). DiI signal was present in the SSLB but not in the plain silica NPs (green, DiI) Scale bar 5 μm. (For interpretation of the references to color in this figure legend, the reader is referred to the web version of this article.)

We proceeded to functionalize SSLBs with anti-EGFR RNA aptamers to determine their cell targeting properties on a panel of breast cancer cell lines (Fig. 4). Two critical NP properties for multivalent targeting are ligand affinity and NP valency, which can be exploited to increase the selectivity towards a specific cell population. Aptamers are ideal for exploring the interplay between affinity and valency thanks to their modular sequence engineering that enables a rapid design of different affinity variants [21]. Furthermore, we investigated the cell targeting of SSLBs based on the differential EGFR density in breast cancer cells, which was reported to have a wide range of densities in the literature [27]. The reported expression levels were confirmed by EGFR labeling and quantification using dSTORM (Fig. S3). Data in Protein Atlas suggests that EGFR has low tissue specificity, and that expression levels in breast cancer tissue are similar to many other cancer tissues [28].

For this study, we synthesized the well described MinE07 anti-EGFR RNA aptamer, here referred to as high affinity (HighAff) aptamer, which binds EGFR with an apparent K_D of 20 nM, as measured in previous work using flow cytometry-based binding assays [21,29]. This sequence was recently engineered to yield a lower affinity aptamer variant, here referred to as low affinity (LowAff), that showed an approximately 6-fold higher apparent K_D of 120 nM (measured using the same cell-based binding assay) [21]. In addition, single-molecule tracking was performed to determine their dissociation rates in the same work. The dissociation rate for the low affinity MinE07_G6U/A33C was estimated at $k_{off} = 4*10^{-2}\ s^{-1}$, while the dissociation rate for MinE07 was too low to measure [21]. While interest in weak affinity ligands seems counterintuitive at first, it makes sense in a NP targeting context, where NP ligands can engage in multivalent interactions with cells and increase the overall binding strength towards cells that present a high receptor expression while weakening their binding towards cells that only present a few copies of that given target receptor.

To functionalize SSLBs for cell targeting, MinE07 aptamers with high and low affinity for EGFR [21,29] were synthesized to bear an anti-overhang sequence (A') at their 3′-ends to facilitate attachment to

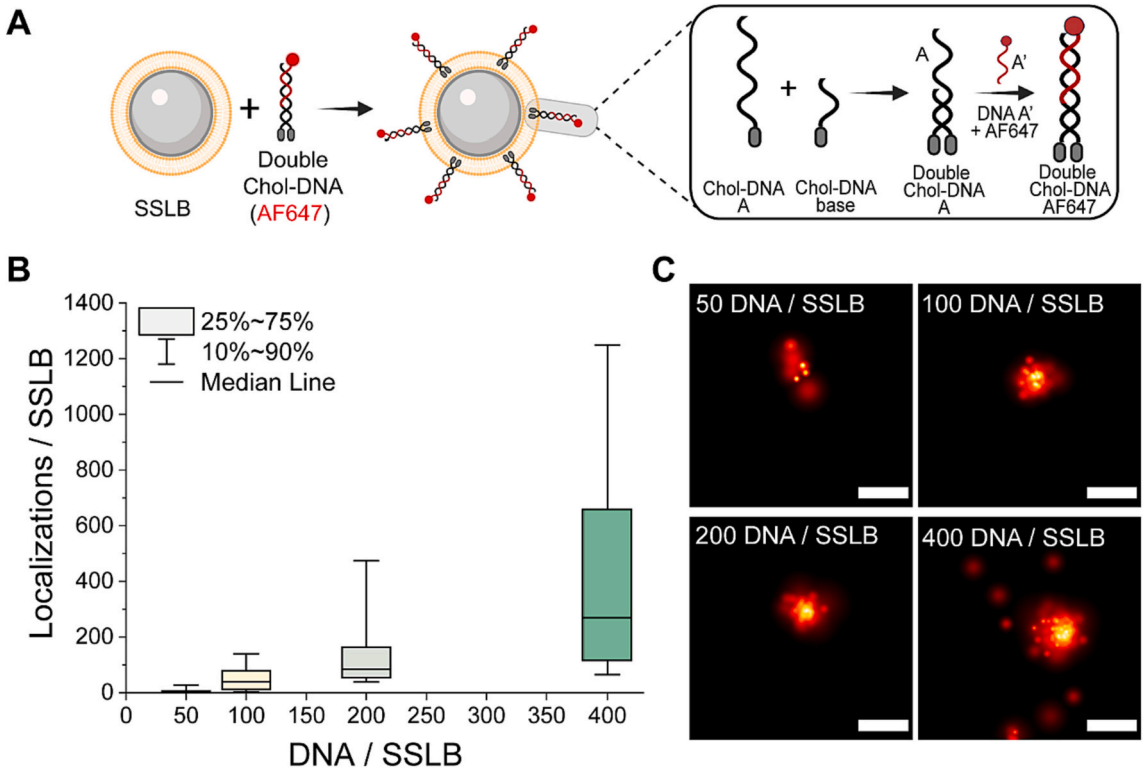

Fig. 3. Quantification of ligand functionalization of SSLB. A) Schematic illustration of double cholesterol-DNA-AF647 linker into the lipid bilayer. Linker molecules were incubated for 1 h with SSLBs at room temperature. The linker is composed of two hybridized cholesterol-DNA strands that form an overhang (A). Ligands containing a complementary sequence (A') can be hybridized to the overhang (A). To quantify the SSLB functionalization with double cholesterol-DNA linkers, a dye molecule was used as a mock ligand. B) dSTORM quantification of different cholesterol-DNA-AF647 molecules inserted into SSLBs at a single-particle level. Minimum 250 particles were quantified per condition C). Representative dSTORM images of SSLB containing different amounts of cholesterol-DNA-AF647 ligands. Scale bar 200 nm.

cholesterol-DNA linkers via DNA hybridization of complementary sequences (between A and A' in this case). Aptamers were then incorporated at different valencies into the SSLBs. Cell targeting was evaluated by reading out the fluorescent silica core signal of SSLBs via flow cytometry assays, giving insight into the interplay between affinity, valency, and EGFR density. Normalized fluorescence intensity histograms were plotted and compared to the signal of cells without SSLB treatment (Fig. 4, grey line). Additionally, the mean fluorescence intensities are shown in Fig. S4. In total, four combinations of SSLBs were tested, namely low and high valency (50 and 400 DNA/SSBL) and low and high-affinity anti-EGFR aptamers (HighAff and LowAff MinE07) in four different breast cancer cell lines with distinct EGFR expression profiles: MDA-MB-468, BT-20, MDA-MB-231 and BT-474 (listed from high to low EGRF expression).

In general, the highest particle targeting across all four cell lines was observed with the high affinity aptamers and high valency SSLBs (Fig. 4). Thus, this formulation presented little discrimination between cells with different cell-surface EGFR densities (Fig. 4, bottom right panel). Cell targeting was also increased at high SSLB valency when using the low-affinity aptamer for low and intermediate-expressing EGFR cells (BT-474, MDA-MB-231 and BT-20). This could be explained by high valency SSLBs also causing an increase in non-specific interactions. There are indeed indications that aptamers, and in general RNA oligonucleotides, can to some extent have non-specific interactions with molecules on the cell surface [21]. These non-specific interactions could be enhanced by having multiple aptamers conjugated to the SSLBs. On the other hand low-affinity aptamer-SSLBs at low valency increased NP targeting only in the high EGFR expressing cells (MDA-MB-468), but not in the other three cell lines that express lower EGFR levels (BT-474, MDA-MB-231 and BT-20). Therefore, targeting to low expressing EGFR cells can be reduced by modulating the SSLB valency.

To further evaluate whether the observed targeting of anti-EGFR aptamer-SSLBs is selective, we determined the cell association of SSLB functionalized with a non-targeting control RNA aptamer (a highly mutated version of MinE07 with a different secondary structure prediction, see Supplementary Table S3). Since the chemical surface environment dictates potential non-specific interactions of SSLBs with cells, it is crucial to compare anti-EGFR SSLBs to a control particle with similar surface chemistry and the same ligand valency. The normalized frequency histograms for non-targeting SSLBs at different valencies are presented in Fig. S5. As a measure for selectivity, the ratio between SSLBs functionalized with an anti-EGFR targeting aptamer compared to the control non-targeting aptamer was calculated and expressed as a fold increase for each cell line (Fig. 5A), keeping the same valency for targeted and non-targeted SSLBs as specified in each condition. Thus, a ratio of 1 would indicate no difference in uptake between EGFR targeting and non-targeting SSLBs (Fig. 5B, grey line), implying that SSLBs are interacting non-specifically with the cells.

At the lowest EGFR density cells (BT-474), the SSLB interaction is mainly non-specific (values around 1), which means there is no discrimination in cell association between targeted and non-targeted SSLBs (Fig. 5B). Consequently, changing SSLB valency or aptamer affinity has no influence on the specificity of SSLB, as the EGFR density is too low to promote significant specific interactions that overcome the non-specific binding contribution. This observation confirms that the increased association of SSLB to BT-474 cells when using HighAff aptamer and high valency (Fig. 4) is largely due to non-specific interactions. Thus, targeted and non-targeted SSLBs with high valency display a similar BT-474 cell binding (Fig. 5 and Fig. S5). This association is significantly reduced by lowering the SSLB valency for both

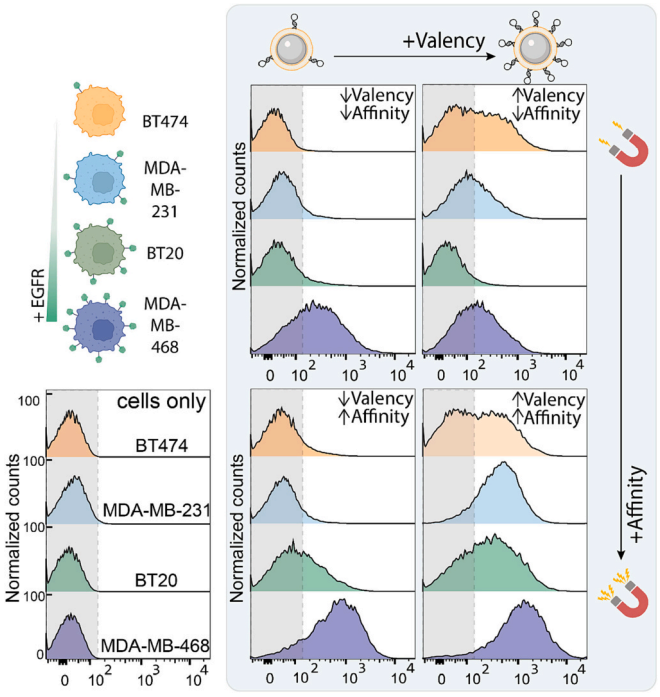

Fig. 4. Targeting of SSLBs with different valency and affinity to a panel of breast cancer cells. SSLBs with low and high valency (50 and 400 DNA/SSBL, respectively) and low and high affinity MinE07 (LowAff and HighAff, respectively) were incubated with breast cancer cell lines of different EGFR density. SSLB internalization was evaluated by flow cytometry, and the normalized frequency was plotted against the fluorescence intensity of the SSLB signal (FITC-labeled silica core). Cells only represent the background cell fluorescence with no SSLB added (grey line). Color code: Orange = BT474, Blue = MDA-MDA-231, Green = BT20 and Purple = MDA-MB-468. Histograms are plotted from low EGFR expressing cells (top) to high EGFR-expressing cells (bottom). (For interpretation of the references to color in this figure legend, the reader is referred to the web version of this article.)

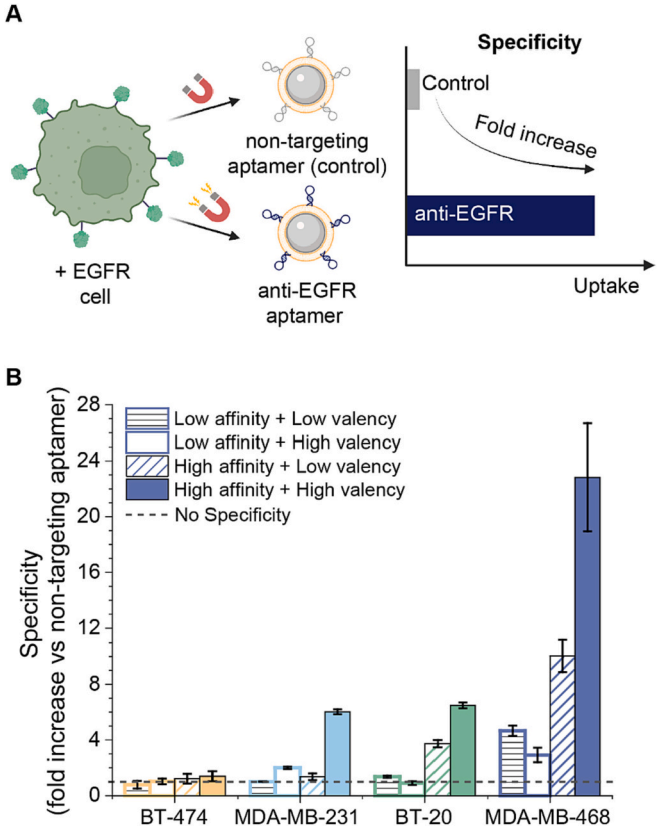

Fig. 5. Targeting specificity of SSLBs determined by flow cytometry. A) Schematic representation of SSLB specificity. SSLBs were functionalized with a scrambled non-targeting aptamer as a control for non-specific NP uptake. The difference in fold increase was measured for the targeting versus the non-targeting SSLBs. B) Fold increase uptake of targeting SSLBs versus non-targeting SSLBs for different formulations and cell lines to determine the specificity of SSLBs. The targeting SSLBs were compared to a control SSLB of the same valency for each cell line. Specificity = 1 is indicated by a dotted line and represents equal uptake of targeted and non-targeted SSLB, indicative of a non-specific interaction. A technical replicate was performed, and the error bars depict the standard deviation derived from the three repetitions.

targeted and non-targeted SSLBs in BT-474 cells, although a discrimination between targeted and non-targeted NPs is not achieved yet.

In the intermediate EGFR density range (MDA-MB-231 and BT-20), cell binding of low affinity SSLBs (with low and high valencies) does not surpass the non-specific background binding shown by the non-targeted SSLBs. In contrast, in MDA-MB-231 cells targeted SSLB association is higher than non-targeted particles only when using high affinity aptamer at the highest valency, while in BT-20 cells improved binding occurs at both low and high valency. This result can be explained by the increased EGFR density in BT-20 cells compared to MDA-MD-231 cells, which results in the formation of an increased number of specific aptamer-EGFR interactions using high-affinity aptamers. Notably, low-affinity aptamers do not show high specificity, probably because the binding affinity is too weak, and multivalent interactions are not favored when cells express intermediate EGFR density levels on their surfaces.

In MDA-MB-468 cells which have a high EGFR density, targeted SSLBs showed an increased cell association compared to non-targeted particles in all tested conditions of aptamer affinity and valency. Notably, a 24-fold increase of targeted SSLB uptake at high affinity and high valency was observed, which could result from multivalent ligand-receptor interactions. These findings show that specificity is an important parameter to consider when tuning the NP valency and affinity, as there is a compromise between maximizing specific association in high-expressing EGFR cells (highest at high valency and affinity) and minimizing the non-specific binding in low-expressing EGFR cells (lowest at low valency and affinity).

Selective NPs are able to distinguish between cells of different receptor densities, favoring the interaction with high over low receptor density cells. To study the selectivity of our aptamer-SSLB formulations, we determined the selectivity ratio. The selectivity ratio is the uptake ratio between cells of a higher EGFR density compared to a cell of a lower EGFR density. Thus, at ratio = 1 we can conclude that there is no difference in SSLB uptake between the two cell types.

We observed a higher selectivity for high EGFR-expressing cells (MDA-MB-468) when compared to the other three breast cancer cell lines (Fig. 6A). This selectivity increases when the difference in receptor expression increases. For example, we observed a maximum of 11-fold increased binding to MDA-MB-468 compared with low-expressing EGFR BT-474 cells, while the increase in cell association was reduced 4-fold in BT-20 cells, as they have closer EGFR levels. In general terms, the highest selectivity ratios are achieved at low valency for high EGFR-expressing MDA-MB-468 cells, with the high-affinity aptamer performing slightly better than the low affinity one in some conditions. Interestingly, low affinity and low valency SSLBs also show high cell specificity compared to non-targeted particles in MDA-MB-468 cells as opposed to the other cell lines (Fig. 5). Although only moderate selectivity was achieved with this formulation, it is an excellent candidate to target specifically high-EGFR expressing cells (MDA-MB-468) while reducing the non-specific uptake contribution in low EGFR-expressing cells. On the other hand, at high valency and low affinity, no selectivity is observed compared to medium and low expressing EGFR cells

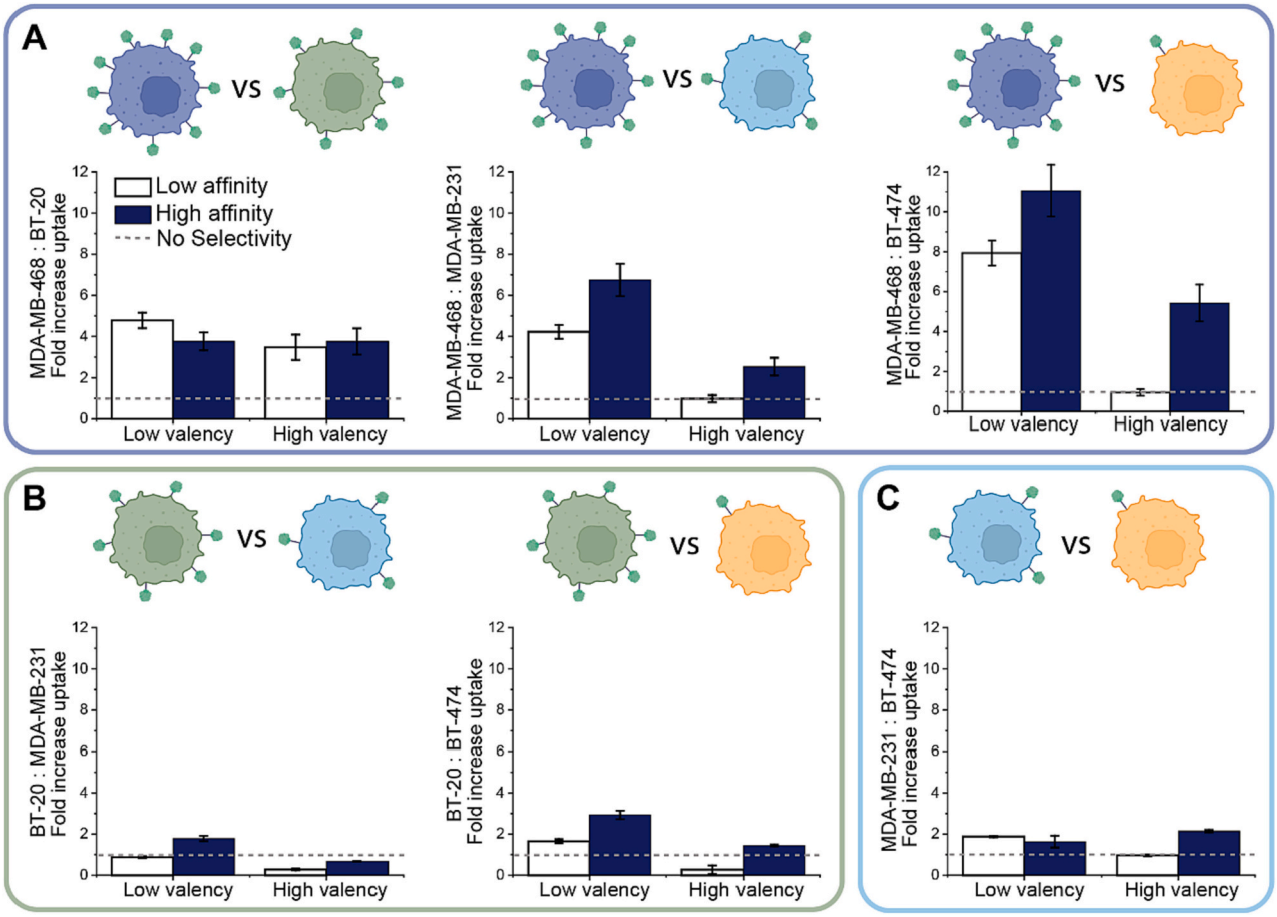

Fig. 6. Targeting selectivity of SSLBs at different aptamer affinity (low = v8 and high = WT) and SSLB valency (low = 50 and high = 400 SSLB/DNA) determined by flow cytometry. Selectivity was expressed as fold increase of fluorescence intensity compared to cell lines of lower EGFR density. Dotted line indicates selectivity = 1 (nonselective uptake) A) MDA-MB-468 selectivity. B) BT-20 selectivity and C) MDA-MB-231 selectivity.

(MDA-MB-231 and BT-474 cells, respectively). As discussed above, this could be related to the higher non-specific binding shown in high valency SSLBs.

Selectively targeting medium expressing EGFR cells compared to low expressing EGFR cells is more challenging (Fig. 6B and C). The highest selectivity was again observed at low valency and high affinity, giving respectively a 2- and 3-fold increased cell binding of BT-20 cells compared to MDA-MB-231 and BT-474 cells. Comparing MDA-MB-231 to BT-474 cells yielded only a 2-fold increase in targeting selectivity at best.

4. Discussion

NP valency and ligand affinity optimization are essential to engineering selective targeted nanomedicines, since on-target off-tumor toxicities often prevent clinical translation of targeted therapeutics [3]. A critical aspect of the rational engineering of NPs is understanding the NP population using single-particle characterization techniques. Here, we used TIRF and dSTORM to elucidate single-particle properties such as lipid bilayer coverage and ligand functionalization. In regard to ligand functionalization, we observed substantial heterogeneity within the same NP population, which was previously described to be present in many NP systems [7,30,31]. This will in turn lead to a heterogeneity in the efficacy of nanoparticles within a population. Thus, single-particle characterization techniques are significant in understanding the NP functionality, which can highly impact their targeting properties and cell uptake. Furthermore, it will be key in the future to develop techniques or methods that enable the production of monodisperse populations of drug nanoparticles.

Recent studies have proven that using more ligands with high affinity does not always lead to an increase in selectivity [3,8,9]. Here, we show that high valency SSLBs functionalized with targeted or non-targeted aptamers leads to increased non-specific binding, thus reducing the selectivity towards high EGFR-expressing cells. Furthermore, there are several downsides to increasing the number of ligands. For example, the steric hindrance of a crowded NP surface can cause a reduction in functionality [11]. At the same time, ligand affinity has become an important parameter in the design of super-selective NPs. Our results suggest that low-affinity ligands are able to interact specifically with high-EGFR expressing cells, while the non-specific uptake with other cell lines is reduced. Studies that combine the NP density and affinity effect on NP uptake are scarce but will significantly improve our understanding of targeting selectivity and the rational design of targeted NPs. For example, Csizmar et al. described that only the reduction of both affinity and valency lead to observable cell selectivity towards cells expressing high levels of the epithelial cell adhesion molecule (EpCAM) [3].

This study uses aptamer-conjugated SSLBs to elucidate the interplay between NP valency, ligand affinity and EGFR expression and its effects on the NP uptake in a panel of EGFR-expressing breast cancer cells with heterogeneous surface EGFR density. Understanding the interplay between these parameters can aid in the formulation of super-selective NPs, that are able to sharply increase their binding towards cells with increased surface receptor density while avoiding low receptor densities, creating a clear on-off binding profile. Aptamers are in many ways preferred ligands over antibodies due to their low immunogenicity and a

smaller size that is reported to be favorable for a more efficient uptake [15]. To illustrate, antibodies can increase the carrier size by roughly 15% for a 200 nm diameter NP, which can also complicate NP diffusion through biological barriers and tissues. Most importantly, aptamers can be synthesized more rapidly and with low batch-to-batch variations and different affinity variants can be engineered, facilitating the understanding of affinity on the selective behavior of multivalent NPs. We observed that the combination of high-affinity aptamers and low valency SSLBs resulted in an increased selectivity towards cells with high EGFR densities. On the other hand, low-affinity aptamers and low valency SSLBs showed lower overall binding to cells with high EGFR density, and cell association is clearly reduced in other cell lines, potentially minimizing the off-tumor targeting. Whether this effect is observed for other cancer cell types expressing EGFR or other cell-targeting aptamers is still not clear and will be further investigated in future studies. In addition, we will determine whether rate of internalization will further impact uptake and selectivity of our targeted NP formulations. In vivo studies would be another key outlook to determine the efficacy of the NP formulations in live tumors.

An exciting outlook of this study is optimizing the lipid composition of SSLBs to enhance cell-specific targeting [32,33]. In fact, in MCF-7 cells, we measured a high cell binding of our SSLBs without aptamers (Fig. S6). For this reason, MCF-7 cells were excluded from further analysis of aptamer affinity and valency to maintain a fair comparison between targeted cell binding of the aptamer-SSLB formulations. Furthermore, ligand mobility is an influential characteristic to achieve selective targeting [34–36]. The lipid composition that we chose to form SSLBs has a natural tendency to be fluid at the studied temperature conditions, potentially allowing the multivalent recruitment of ligands by redirecting them from the distal face of the NP towards the cell surface upon initial cell receptor binding [37]. Whether the formulations retain their fluidity upon ligand functionalization, and what effect the lipid composition has on cell selectivity remains to be explored in further studies.

5. Conclusion

Multivalent interactions between various ligand-receptor pairs can be explored to increase selective NP targeting towards the cells of interest. In this work, we proposed aptamers of tunable affinity conjugated to SSLBs to explore the relationships among NP valency, ligand affinity, and cell receptor density. Using dSTORM, we showed that ligand functionalization of SSLBs using cholesterol-DNA anchors follows a linear trend with increasing amounts of ligands added, and interparticle heterogeneity can be quantified at the single-particle level. Furthermore, tuning NP valency and aptamer affinity can maximize the specificity and selectivity of SSLBs. This was tested in a range of breast cancer cell lines presenting different EGFR densities. We show that using high valency SSLBs resulted in reduced selectivity towards high EGFR density cells compared to their low valency counterparts, in part due to the high non-specific binding of low expressing EGFR cells that arises from having higher ligand copies on the particle surface. In contrast, NPs decorated with a lower amount (low valency) of high affinity ligands bind specifically to high-EGFR expressing cells, while the non-specific association with the other investigated cell lines is reduced. We believe that tuning ligand affinity and NP density will contribute to the rational design of more selective targeted NPs.

Supplementary data to this article can be found online at https://doi.org/10.1016/j.jconrel.2023.01.008.

CRediT authorship contribution statement

Laura Woythe: Conceptualization, Methodology, Investigation, Writing – original draft. **David Porciani:** Methodology, Investigation. **Tessa Harzing:** Investigation. **Stijn van Veen:** Investigation. **Donald H. Burke:** Conceptualization, Writing – review & editing, Supervision, Funding acquisition. **Lorenzo Albertazzi:** Conceptualization, Writing – review & editing, Supervision, Funding acquisition.

Declaration of Competing Interest

None.

Data availability

Data will be made available on request.

Acknowledgements

This work was financially supported by the Netherlands Science Organization (Grant 192.028) through the VIDI program, the European Union's Horizon 2020 research and innovation program under the European Research Council grant ERC-StG-757397 (NANOSTORM), the MU Life Sciences Center (LSC) - Early Concept Grant (ECG) 2019 for Innovative Collaborative Research involving Post-Doctoral Researchers (PI: Burke-Daniels-Porciani), and the UM Research and Creative Works Strategic Investment Program grant (PI: Burke).

References

[1] L. Woythe, N.B. Tito, L. Albertazzi, A quantitative view on multivalent nanomedicine targeting, Adv. Drug Deliv. Rev. 169 (2021) 1–21, https://doi.org/10.1016/j.addr.2020.11.010.
[2] Z. Cheng, A. Al Zaki, J.Z. Hui, V.R. Muzykantov, A. Tsourkas, Multifunctional nanoparticles: cost versus benefit of adding targeting and imaging capabilities, Science. 338 (2012) 903–910, https://doi.org/10.1126/science.1226338.
[3] C.M. Csizmar, J.R. Petersburg, T.J. Perry, L. Rozumalski, B.J. Hackel, C.R. Wagner, Multivalent ligand binding to cell membrane antigens: defining the interplay of affinity, valency, and expression density, J. Am. Chem. Soc. 141 (2019) 251–261, https://doi.org/10.1021/jacs.8b09198.
[4] T. Curk, J. Dobnikar, D. Frenkel, Design principles for super selectivity using multivalent interactions, in: J. Huskens, L.J. Prins, R. Haag, B.J. Ravoo (Eds.), Multivalency, John Wiley & Sons, Ltd, Chichester, UK, 2017, pp. 75–101, https://doi.org/10.1002/9781119143505.ch3.
[5] T. Curk, J. Dobnikar, D. Frenkel, Optimal multivalent targeting of membranes with many distinct receptors, Proc. Natl. Acad. Sci. U. S. A. 114 (2017) 7210–7215, https://doi.org/10.1073/pnas.1704226114.
[6] F.J. Martinez-Veracoechea, D. Frenkel, Designing super selectivity in multivalent nano-particle binding, Proc. Natl. Acad. Sci. 108 (2011) 10963–10968, https://doi.org/10.1073/pnas.1105351108.
[7] L. Woythe, P. Madhikar, N. Feiner-Gracia, C. Storm, L. Albertazzi, A single-molecule view at nanoparticle targeting selectivity: correlating ligand functionality and cell receptor density, ACS Nano (2022), https://doi.org/10.1021/acsnano.1c08277 acsnano.1c08277.
[8] M.R.W. Scheepers, L.J. van IJzendoorn, M.W.J. Prins, Multivalent weak interactions enhance selectivity of interparticle binding, Proc. Natl. Acad. Sci. U. S. A. 117 (2020) 22690–22697, https://doi.org/10.1073/pnas.2003968117.
[9] C. Linne, D. Visco, S. Angioletti-Uberti, L. Laan, D.J. Kraft, Direct visualization of superselective colloid-surface binding mediated by multivalent interactions, Proc. Natl. Acad. Sci. U. S. A. 118 (2021), e2106036118, https://doi.org/10.1073/pnas.2106036118.
[10] L. Albertazzi, F.J. Martinez-Veracoechea, C.M.A. Leenders, I.K. Voets, D. Frenkel, E.W. Meijer, Spatiotemporal control and superselectivity in supramolecular polymers using multivalency, Proc. Natl. Acad. Sci. 110 (2013) 12203–12208, https://doi.org/10.1073/pnas.1303109110.
[11] A.M. Alkilany, L. Zhu, H. Weller, A. Mews, W.J. Parak, M. Barz, N. Feliu, Ligand density on nanoparticles: a parameter with critical impact on nanomedicine, Adv. Drug Deliv. Rev. 143 (2019) 22–36, https://doi.org/10.1016/j.addr.2019.05.010.
[12] B. Powell Gray, S. Li, K.C. Brown, From phage display to nanoparticle delivery: functionalizing liposomes with multivalent peptides improves targeting to a cancer biomarker, Bioconjug. Chem. 24 (2013) 85–96, https://doi.org/10.1021/bc300498d.
[13] J. Wang, J. Min, S.A. Eghtesadi, R.S. Kane, A. Chilkoti, Quantitative study of the interaction of multivalent ligand-modified nanoparticles with breast cancer cells with tunable receptor density, ACS Nano 14 (2020) 372–383, https://doi.org/10.1021/acsnano.9b05689.
[14] P. Kalra, A. Dhiman, W.C. Cho, J.G. Bruno, T.K. Sharma, Simple methods and rational design for enhancing aptamer sensitivity and specificity, Front. Mol. Biosci. 5 (2018) 41, https://doi.org/10.3389/fmolb.2018.00041.
[15] S. Zununi Vahed, N. Fathi, M. Samiei, S. Maleki Dizaj, S. Sharifi, Targeted cancer drug delivery with aptamer-functionalized polymeric nanoparticles, J. Drug Target. 27 (2019) 292–299, https://doi.org/10.1080/1061186X.2018.1491978.
[16] K.S. Butler, P.N. Durfee, C. Theron, C.E. Ashley, E.C. Carnes, C.J. Brinker, Protocells: modular mesoporous silica nanoparticle-supported lipid bilayers for

drug delivery, Small. 12 (2016) 2173–2185, https://doi.org/10.1002/smll.201502119.
[17] M. Rinaldin, Colloid supported lipid bilayers for self-assembly, Soft Matter 15 (2019) 1345–1360, https://doi.org/10.1039/C8SM01661E.
[18] E.C. Giakoumatos, Hard Colloids and Soft Interfaces, Technische Universiteit Eindhoven, 2020.
[19] A. Jimenez, K. Friedl, C. Leterrier, About samples, giving examples: optimized single molecule localization T microscopy, Methods. 174 (2020) 100–114.
[20] N. Feiner-Gracia, M. Beck, S. Pujals, S. Tosi, T. Mandal, C. Buske, M. Linden, L. Albertazzi, Super-resolution microscopy unveils dynamic heterogeneities in nanoparticle protein corona, Small. 13 (2017) 1701631, https://doi.org/10.1002/smll.201701631.
[21] P. Delcanale, D. Porciani, S. Pujals, A. Jurkevich, A. Chetrusca, K.D. Tawiah, D. H. Burke, L. Albertazzi, Aptamers with tunable affinity enable single-molecule tracking and localization of membrane receptors on living cancer cells, Angew. Chem. Int. Ed. 59 (2020) 18546–18555, https://doi.org/10.1002/anie.202004764.
[22] S. Mornet, O. Lambert, E. Duguet, A. Brisson, The formation of supported lipid bilayers on silica nanoparticles revealed by cryoelectron microscopy, Nano Lett. 5 (2005) 281–285, https://doi.org/10.1021/nl048153y.
[23] S.A.J. van der Meulen, G.V. Dubacheva, M. Dogterom, R.P. Richter, M. E. Leunissen, Quartz crystal microbalance with dissipation monitoring and spectroscopic ellipsometry measurements of the phospholipid bilayer anchoring stability and kinetics of hydrophobically modified DNA oligonucleotides, Langmuir. 30 (2014) 6525–6533, https://doi.org/10.1021/la500940a.
[24] I. Pfeiffer, F. Höök, Bivalent cholesterol-based coupling of oligonucletides to lipid membrane assemblies, J. Am. Chem. Soc. 126 (2004) 10224–10225, https://doi.org/10.1021/ja048514b.
[25] M.J. Rust, M. Bates, X. Zhuang, Sub-diffraction-limit imaging by stochastic optical reconstruction microscopy (STORM), Nat. Methods 3 (2006) 793–796, https://doi.org/10.1038/nmeth929.
[26] M. Lelek, M.T. Gyparaki, G. Beliu, F. Schueder, J. Griffié, S. Manley, R. Jungmann, M. Sauer, M. Lakadamyali, C. Zimmer, Single-molecule localization microscopy, Nat. Rev. Methods Prim. 1 (2021) 39, https://doi.org/10.1038/s43586-021-00038-x.
[27] H. Zou, M.B. Sevigny, S. Liu, D.T. Madden, M.C. Louie, Novel flexible heteroarotinoid, SL-1-39, inhibits HER2-positive breast cancer cell proliferation by promoting lysosomal degradation of HER2, Cancer Lett. 443 (2019) 157–166, https://doi.org/10.1016/j.canlet.2018.11.022.
[28] Expression of EGFR in cancer - Summary - The Human Protein Atlas. https://www.proteinatlas.org/ENSG00000146648-EGFR/pathology, 2022 (accessed November 18, 2022).
[29] N. Li, H.H. Nguyen, M. Byrom, A.D. Ellington, Inhibition of cell proliferation by an anti-EGFR aptamer, PLoS One 6 (2011), e20299, https://doi.org/10.1371/journal.pone.0020299.
[30] T. Andrian, P. Delcanale, S. Pujals, L. Albertazzi, Correlating super-resolution microscopy and transmission electron microscopy reveals multiparametric heterogeneity in nanoparticles, Nano Lett. (2021), https://doi.org/10.1021/acs.nanolett.1c01666 acs.nanolett.1c01666.
[31] D.G. Mullen, E.L. Borgmeier, M. Fang, D.Q. McNerny, A. Desai, J.R. Baker, B. G. Orr, M.M. Banaszak Holl, Effect of mass transport in the synthesis of partially acetylated dendrimer: implications for functional ligand−nanoparticle distributions, Macromolecules. 43 (2010) 6577–6587, https://doi.org/10.1021/ma100663c.
[32] H. Abumanhal-Masarweh, D. da Silva, M. Poley, A. Zinger, E. Goldman, N. Krinsky, R. Kleiner, G. Shenbach, J.E. Schroeder, J. Shklover, J. Shainsky-Roitman, A. Schroeder, Tailoring the lipid composition of nanoparticles modulates their cellular uptake and affects the viability of triple negative breast cancer cells, J. Control. Release 307 (2019) 331–341, https://doi.org/10.1016/j.jconrel.2019.06.025.
[33] M.P. Lokugamage, D. Vanover, J. Beyersdorf, M.Z.C. Hatit, L. Rotolo, E. S. Echeverri, H.E. Peck, H. Ni, J.-K. Yoon, Y. Kim, P.J. Santangelo, J.E. Dahlman, Optimization of lipid nanoparticles for the delivery of nebulized therapeutic mRNA to the lungs, Nat. Biomed. Eng. 5 (2021) 1059–1068, https://doi.org/10.1038/s41551-021-00786-x.
[34] S. Maslanka Figueroa, D. Fleischmann, S. Beck, A. Goepferich, The effect of ligand mobility on the cellular interaction of multivalent nanoparticles, Macromol. Biosci. 20 (2020) 1900427, https://doi.org/10.1002/mabi.201900427.
[35] G.V. Dubacheva, T. Curk, B.M. Mognetti, R. Auzély-Velty, D. Frenkel, R.P. Richter, Superselective targeting using multivalent polymers, J. Am. Chem. Soc. 136 (2014) 1722–1725, https://doi.org/10.1021/ja411138s.
[36] L. Wu, H. Ding, X. Qu, X. Shi, J. Yang, M. Huang, J. Zhang, H. Zhang, J. Song, L. Zhu, Y. Song, Y. Ma, C. Yang, Fluidic multivalent membrane nanointerface enables synergetic enrichment of circulating tumor cells with high efficiency and viability, J. Am. Chem. Soc. 142 (2020) 4800–4806, https://doi.org/10.1021/jacs.9b13782.
[37] C.E. Ashley, E.C. Carnes, G.K. Phillips, D. Padilla, P.N. Durfee, P.A. Brown, T. N. Hanna, J. Liu, B. Phillips, M.B. Carter, N.J. Carroll, X. Jiang, D.R. Dunphy, C. L. Willman, D.N. Petsev, D.G. Evans, A.N. Parikh, B. Chackerian, W. Wharton, D. S. Peabody, C.J. Brinker, The targeted delivery of multicomponent cargos to cancer cells by nanoporous particle-supported lipid bilayers, Nat. Mater. 10 (2011) 389–397, https://doi.org/10.1038/nmat2992.